Effect of Relative Humidity on OH Uptake by Surfaces of Atmospheric Importance

ARTICLE *in* THE JOURNAL OF PHYSICAL CHEMISTRY A · AUGUST 2008

Impact Factor: 2.69 · DOI: 10.1021/jp8012317 · Source: PubMed

3 AUTHORS, INCLUDING:

Jong-Ho Park
Korea Atomic Energy Research Institute (K…
34 PUBLICATIONS **191** CITATIONS
SEE PROFILE

Andrey V Ivanov
University of California, San Diego
61 PUBLICATIONS **626** CITATIONS
SEE PROFILE

Effect of Relative Humidity on OH Uptake by Surfaces of Atmospheric Importance

Jong-Ho Park,† Andrey V. Ivanov,* and Mario J. Molina

Department of Chemistry and Biochemistry, University of California-San Diego, La Jolla, California 92039

Received: February 11, 2008; Revised Manuscript Received: May 6, 2008

An experimental study of the dependence of the OH uptake coefficient γ_{OH} over a relative humidity of 0−48% was carried out at 100 Torr and room temperature, using a differential bead-filled flow tube coupled to a high-pressure chemical ionization mass spectrometer. Various organic (paraffin wax, pyrene, glutaric acid, and soot) and inorganic (NaCl, KCl, $MgCl_2$, $CaCl_2$, Na_2SO_4, and sea salt) surfaces served as proxies for tropospheric aerosols. A virtual cylindrical flow tube approximation and a surface coating dilution technique were successfully employed in the study, which included measurements of high radical uptake with an initial probability of near unity. For inorganic salts, the effect of water vapor, enhancement or inhibition of γ_{OH}, was found to be dependent on the blocking of anions and changes in surface pH. Although OH uptake by NaCl, the major component of sea-salt aerosols, is weakly dependent on water vapor, it is enhanced by a factor of ∼2 for $MgCl_2$ and determines the net relative humidity dependence of the radical uptake on sea salt, which is enhanced by a factor of ∼4. For the organic surfaces studied, the enhancement effect of a factor 4 was also observed only for a hydrophilic organic surface, namely, glutaric acid. Results of the uptake studies suggest that the effect of relative humidity is important and should be accounted for in atmospheric modeling of tropospheric aerosol chemistry.

Introduction

Despite its short atmospheric lifetime, heterogeneous reactions of OH are now recognized to be important due to their ability to initiate oxidation of organic particulates,[1–5] to react with inorganic aerosols modifying their physical and chemical properties (aging),[6–16] to enhance heterogeneous oxidation of sulfur,[17–19] to produce photochemically active halogen products that are released to the gas phase,[20–25] and to determine cloud chemistry to a significant extent.[26,27,29–31] At an average OH concentration of $\sim 10^6$ molecule cm^{-3} in the troposphere,[32,33] radical uptake often becomes the rate-determining step for the entire process of physicochemical transformation of aerosol particles. Atmospheric modeling of aerosol chemistry is to a large extent constrained by the very limited chemical kinetics data on the uptake of radicals.[6–9] In addition, most uptake measurements have been carried out under dry conditions whereas water vapor is one of the major gas components of the troposphere.[34,35]

Due to its relatively large dipole moment[36] and ability to form strong hydrogen bonds, water molecules are taken up efficiently by surfaces with high surface tension. Adsorbed water is, in general, capable of either inhibiting or enhancing OH uptake by modifying the nature of the active surface sites, and thus it can lead to reaction mechanisms of radical capture by the surface different from those that are specific to dry conditions. For instance, carbonaceous surfaces exposed to OH become hydrophilic with increased water adsorption capacity.[1,37] On the other hand, a water adlayer can either block active sites from further reactions with hydroxyl radicals or enhance the chemical reactivity of active sites by increasing their coordination number and causing their partial dissociation. For inorganic surfaces, adsorbed water can significantly enhance the surface ionic mobility affecting ionic concentrations within the surficial layer[38] as well as altering the pH of an aerosol surface which will affect the OH uptake rate. Segregation of halide ions observed to be present at the surface of sea-salt particles under high humidity conditions was found to be most likely a key step in the formation of gas-phase halogen-containing products.[20,21]

There is practically no information in the literature directly measuring OH uptake by aerosol surfaces under high humidity conditions. Our group has carried out the only study[2] on OH uptake by organic surfaces in which the uptake coefficient was directly measured at low pressure in the presence of water vapor, but the relative humidity (RH) was less than 1% in that study. The results of that study showed that the OH uptake coefficient is independent of the presence of water vapor for initially hydrophobic organic surfaces, such as aliphatics, aromatics, and soot. OH uptake measurements for deliquesced sea salt and its individual components have been carried out at an RH of 80% and higher.[14,20,21] The results of these indirect measurements indicated noticeable enhancement in the OH uptake rate on the surfaces exposed to water vapor.

In the present work a new approach has been developed and used to explore experimentally the effect of relative humidity on OH uptake by various organic and inorganic surfaces and its relevance to tropospheric chemistry. This new approach is based on a virtual flow tube approximation and a surface dilution technique that allow measurements of radical uptake with an initial probability near unity at high pressure and relative humidity.

Experimental Section

Experimental studies in the present work were performed under flow conditions at 100 Torr and room temperature, using the setup shown schematically in Figure 1. The setup consisted of a fast flow system, which included an OH generator and a

* Author to whom correspondence should be addressed. E-mail: avivanov@ucsd.edu..

† Also affiliated with: Department of Chemistry, Massachusetts Institute of Technology, Cambridge, MA 02139.

10.1021/jp8012317 CCC: $40.75
Published on Web 07/02/2008

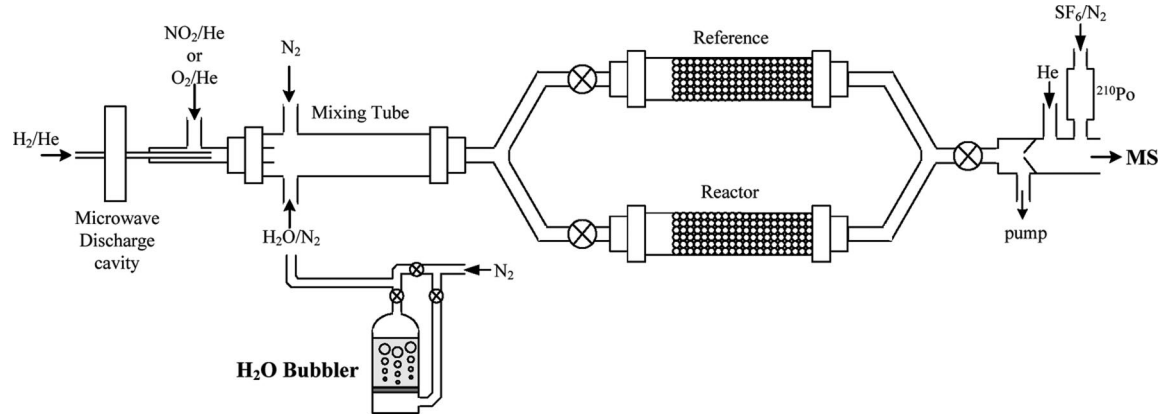

Figure 1. Schematic diagram of the differential flow tube coupled to CIMS.

differential flow tube, coupled to a high-pressure chemical ionization mass spectrometer (CIMS). The OH generator section in the figure shows different methods of OH production. For the uptake studies, a NO_x-free source of OH was used to avoid heterogeneous reactions of nitrogen oxides that would possibly modify the surface. In this case the following reactions in an excess of H over HO_2 were employed for OH production at 100 Torr:

$$H + O_2 + M \rightarrow HO_2 + M$$

$$k = 1.9 \times 10^{-13}\ \text{cm}^3\ \text{molecule}^{-1}\ \text{s}^{-1}\ ^{39} \quad (1)$$

$$H + HO_2 \rightarrow OH + OH$$

$$k = 7.2 \times 10^{-11}\ \text{cm}^3\ \text{molecule}^{-1}\ \text{s}^{-1}\ ^{40} \quad (2)$$

Molecular hydrogen diluted ~1000-fold in helium (UHP, Airgas) was used to generate hydrogen atoms of $\sim 10^{12}$ molecule cm^{-3} in a Beenaker microwave cavity operated at 30 W. H atoms were mixed downstream with an excess of O_2 (UHP, Airgas) at $\sim 10^{13}$ molecule cm^{-3} in a 0.4 cm i.d. tube to form OH. To minimize the contribution of the OH self-reaction, the radical-containing flow was expanded to a larger 0.95 cm i.d. tube in which it was additionally diluted with N_2 (UHP, Praxair) consisting of a main carrier gas flow and a flow with saturated water vapor. The difference in pressures of high humidity and dry N_2 flows was used to estimate relative humidity; accuracy of relative humidity determination is within 1.5% of RH. The diluted flow was then introduced into a differential flow tube that consisted of two identical 0.95 cm Pyrex tubes, reference and reaction, with the possibility of switching the flow between them. Each flow tube was filled with 60 glass beads coated with halocarbon wax or with the material of interest. After passing through the differential flow tube, the remaining OH entered the chemical ionization region via a 1 mm skimmer for titration with SF_6^- ions that were produced by passing SF_6 (Matheson Tri Gas, 99.99%) diluted in N_2 through a ^{210}Po source (NRD), by the following reaction:

$$OH + SF_6^- \rightarrow OH^- + SF_6$$

$$k = 1.7 \times 10^{-9}\ \text{cm}^3\ \text{molecule}^{-1}\ \text{s}^{-1} \quad (3)$$

The value of the rate constant for this reaction was estimated using the average dipole orientation theory.[41]

The OH^- ions were detected by a quadrupole mass spectrometer after entering via a 0.1 mm pinhole biased at −5 V to a chamber pumped differentially by two turbo molecular pumps (Leybold 360CSV, Seiko-Seiki STP-400). A series of ion optics further focused the ions to increase the sensitivity of the mass spectrometer.

Water vapor affects radical detection, specifically in the chemical ionization region, reducing the CIMS sensitivity to OH due to efficient formation of water clusters with both the SF_6^- parent ion producing $SOF_4^-\cdot(H_2O)_m$ and $F^-\cdot(HF)_2\cdot(H_2O)_n$ and with the OH^- reagent ion producing $OH^-\cdot(H_2O)_k$ at high pressure.[42,43] Although dilution with He and lowering the pressure inside the chemical ionization region can help decluster the water complexes, it is still necessary to calibrate the OH signal as a function of RH. For this purpose, as is well established, the OH signal, produced by the following fast reaction,

$$H + NO_2 \rightarrow OH + NO$$

$$k = 1.3 \times 10^{-10}\ \text{cm}^3\ \text{molecule}^{-1}\ \text{s}^{-1}\ ^{38} \quad (4)$$

was calibrated by introducing known amounts of NO_2 (Matheson Tri Gas, 99.5%). The CIMS detection limits to OH were determined to be 4×10^7, 4×10^8, and 4.5×10^9 molecule cm^{-3} at 100 Torr and RH = 0, 6, and 48%, respectively, with S/N = 1 and a 0.5 s integration time. The initial OH signal-to-noise ratio is about 10^4 under dry conditions, which decreased by 2 orders of magnitude to 10^2 as the RH was raised to 48%. Obviously such relatively low detection limits result in larger experimental errors in R and, therefore, in γ.

To prevent radical wall losses, the differential flow tube and glass connections of gas lines were coated with halocarbon wax (series 600, Halocarbon Inc.). The flow rates were monitored with calibrated electronic mass flow meters (Tylan), and pressure in the differential flow tube was measured with an absolute pressure gauge (MKS 1000, Baratron).

Because the OH diffusion coefficient in H_2O is close to that in N_2,[27,44] the carrier gas, the presence of water vapor in the differential flow tube caused negligible changes in the net OH diffusion coefficient, namely less than 2% at RH = 50%.

Glass beads were first cleaned with sulfuric acid, rinsed with deionized water, and dried in an oven at 400 K for half an hour. The beads in the reference tube were coated with halocarbon wax, whereas those in the reactor were coated with the organic or inorganic materials of interest.

Pure organic coatings, such as halocarbon wax, paraffin wax (J. T. Baker), pyrene (Sigma-Aldrich, 99.5%), and glutaric acid (Sigma-Aldrich, 99%), were prepared by melting the solid material, covering the glass beads with the resulting liquid, and then letting the liquid solidify at room temperature. Melting temperatures were controlled to prevent decomposition or oxidation of the organic material. Figure 2 shows optical

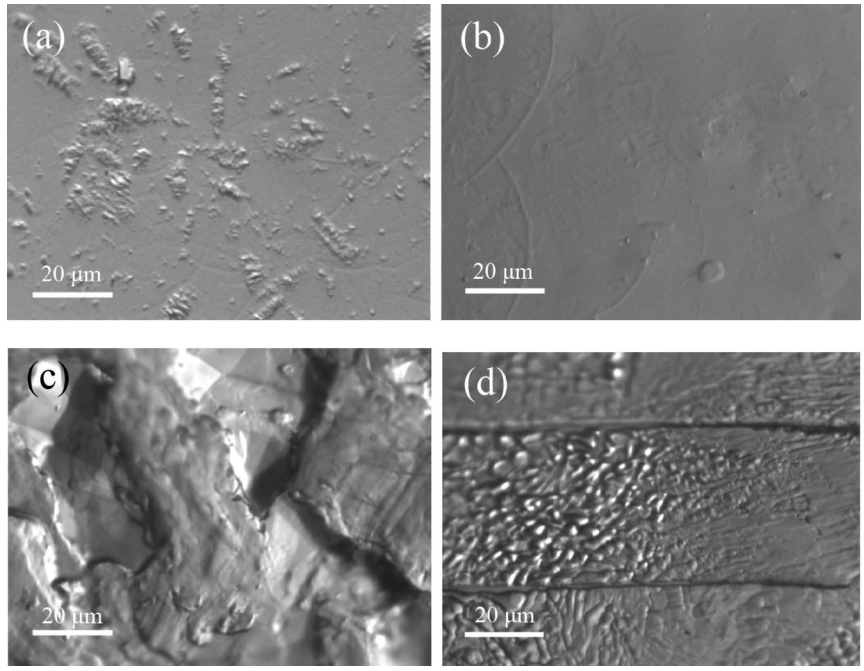

Figure 2. Optical images of bare glass (a), halocarbon (b) and paraffin (c) waxes, and glutaric acid (d).

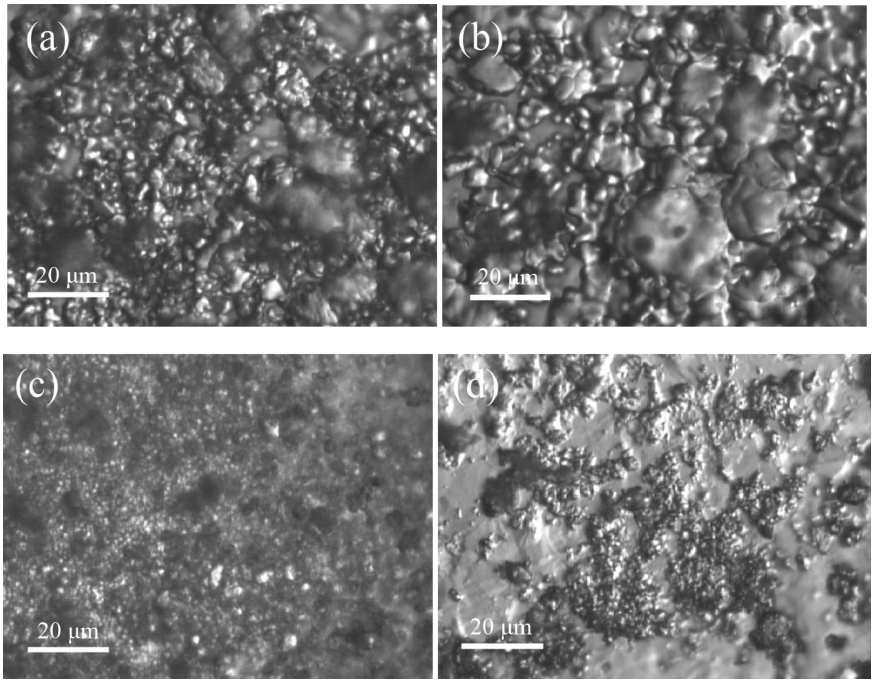

Figure 3. Optical microscopic images of NaCl (a), KCl (b), SiO_2 (c), and Al_2O_3 (d).

microscopic images of bare glass beads and beads coated with pure halocarbon wax, paraffin wax, and glutaric acid were acquired with a Zeiss Axioskop 20 microscope equipped with 10× or 50× objectives for the quality control of the coatings.

To get thin homogeneous inorganic (salt and mineral) coatings on the spherical surfaces, the following technique was used: first, glass beads were coated with halocarbon wax as described above; then, the pre-coated sticky beads were shaken vigorously with fine powder of the inorganic material in a Petri dish. The quality of the coatings was again monitored with optical microscopy. Figure 3 shows optical microscopic images for the selected inorganic surfaces. The inorganic materials studied in this work were $CaCl_2$ dihydrate (Mallinckrodt, 99%), NaCl (Mallinckrodt, 99.9%), KCl (Fisher Scientific, ACS grade), $MgCl_2$ (Sigma-Aldrich, 99.5%), $MgSO_4$ (Sigma-Aldrich, 99.9%), Na_2SO_4 (Sigma-Aldrich, ≥99.0%), sea salt (Sigma-Aldrich), SiO_2 (Sigma-Aldrich, 99.6%), and Al_2O_3 (Sigma-Aldrich, 99.9%).

The soot coatings were prepared in the same way as the inorganic coatings; soot samples were collected from a methane−air flame produced from a standard Bunsen burner without any additional control of an air−fuel ratio. Previous studies in our group have shown that methane soot surfaces are initially hydrophobic.[1,2,37]

For preparation of diluted surface coatings with less reactivity, organic and inorganic materials were mixed with halocarbon wax and then the previously described techniques were used for the final coating (see the Results and Discussion for details).

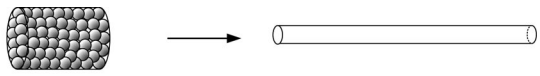

$V = \pi r^2 L - (4/3)\pi r_b^3 N$
$S = 4\pi r_b^2 N$

$r_v = 2V/S$
$l_v = V/(\pi r_v^2)$
$t = Vp/W$

Figure 4. Conversion of a flow tube packed with beads to a virtual cylindrical flow tube.

Results and Discussion

Determination of the uptake coefficient, γ, was based on measurements of the OH signal with the radical-containing flux entering the *reaction* flow tube and measurements of the signal with the radicals flowing through the *reference* flow tube. In each case the signal is proportional to the amount of OH remaining after the heterogeneous reaction with the bead-surface coating, and therefore, it is determined by the OH uptake coefficient. Previous studies have shown that, for most of the surfaces studied here, heterogeneous OH loss is first order[1,6–9] and can be described as follows:

$$\mathrm{OH} + \mathrm{surface} \rightarrow \mathrm{loss} \qquad k_{het} \tag{5}$$

and

$$[\mathrm{OH}]_t = [\mathrm{OH}]_0 \exp(-k_{het} t) \tag{6}$$

where $[\mathrm{OH}]_0$ and $[\mathrm{OH}]_t$ are the gas-phase OH concentrations before and after reaction with the bead surface, respectively, (molecule cm^{-3}); k_{het} is the pseudo-first-order rate constant for heterogeneous OH loss (s^{-1}); and t is the OH residence time for reaction with the bead surface (in seconds).

In our experiments the ratio between the reaction and reference OH signals, R, is given by the following expression:

$$R = \frac{\mathrm{OH}_t^{\mathrm{react}}}{\mathrm{OH}_t^{\mathrm{ref}}} = \exp\left[-\left(k_{het}^{\mathrm{react}} - k_{het}^{\mathrm{ref}}\right)t\right] \tag{7}$$

To estimate k_{het} and t, we utilized an approximation replacing the bead-filled reactor with a virtual cylindrical flow tube, as described in the next section.

Vrtual Cylindrical Flow Tube Approximation. The flow tubes used in the present study were packed with beads for two reasons: to increase the surface area available for the heterogeneous reaction and to shorten the OH diffusion time to the surface. In the virtual cylindrical flow tube (VCFT) approximation, the flow tube packed with beads is replaced with a cylindrical flow tube with a radius r_v and a length l_v chosen so that the tube has the same surface area as the beads, S, and a volume equal to the space between the beads, V. The geometric parameters for the virtual cylindrical flow tube are calculated as follows:

$$S = 4\pi r_b^2 N \tag{8}$$

$$V = \pi r^2 L - 4/3\pi r_b^3 N \tag{9}$$

$$r_v = 2V/S \tag{10}$$

$$l_v = V/(\pi r_v^2) \tag{11}$$

where $r_b = 0.15 \pm 0.01$ cm is the bead radius, $N = 60$ is the number of beads, $r = 0.47 \pm 0.01$ cm is the radius of the reference/reaction flow tube packed with beads, and $L = 2.6 \pm 0.1$ cm is the length of the bead packing in the differential flow tube (see Figure 4). These parameters give a virtual flow tube volume (V) of 1.01 cm^3. Therefore, the residence time inside the virtual cylindrical flow tube is determined as follows:

$$t = \frac{l_v}{v} = \frac{Vp}{W} \tag{12}$$

where v is the gas convective velocity with a total flow W (at 1 Torr) and p is the pressure in the differential flow tube. Under typical experimental conditions $v = 7.3 \times 10^3$ cm s^{-1} and $W = 3.4 \times 10^4$ cm^3 Torr s^{-1}. A pressure of 100 Torr gives a residence time in the virtual flow tube of ~3 ms. The Reynolds number for the virtual flow tube was calculated to be 1300, suggesting a laminar flow. However, it should be noted that this value is inappropriate to describe the flow regime in a flow tube packed with beads.

In addition to the geometric parameters S and V, it is necessary to verify that the OH diffusion time to the surface was not changed in the VCFT approximation. We did this by estimating the average distance traveled by OH to the surface of the beads and comparing it to the radius of the VCFT. Using an equal-sided pyramid to approximate the space between beads in regular close-packing, we estimated that the sides of the pyramids are, on average, close to the diameter of the virtual cylindrical flow tube calculated from eq 10. Consequently, we were able to estimate the average distance traveled by OH to the surface. No noticeable differences were found between the bead-filled cylindrical flow tube and the virtual cylindrical tube, showing that the VCFT approximation accurately reproduces flow conditions in the real bead-filled flow tube.

Under laminar conditions, the first-order rate constant of heterogeneous OH loss in a cylindrical flow tube can be determined from the additivity of kinetic resistances[45]

$$\frac{1}{k_{het}} = \frac{1}{k_{kin}} + \frac{1}{k_{dif}} \tag{13}$$

where k_{kin} and k_{dif} are the kinetic and diffusive limits of k_{het}, respectively, and relate to the uptake coefficient and the diffusion coefficient in the following way:

$$k_{kin} = \frac{2\gamma}{2-\gamma}\frac{\omega}{2r_v} \tag{14}$$

and

$$k_{dif} = 3.67\frac{D_p}{r_v^2} \tag{15}$$

where γ is the uptake coefficient, defined as the ratio of the measured overall flux of gas to the surface to the kinetic collision rate per unit of surface area,[46] ω is the average thermal velocity (cm s^{-1}) of the radicals, and D_p is the gaseous diffusion coefficient at pressure p in the differential flow tube (cm^2 s^{-1}).

Using eqs 8–15, the R ratio can be finally expressed as follows

$$R = \exp\left[-\left(\frac{k_{kin}^{\mathrm{react}} k_{dif}^{\mathrm{react}}}{k_{kin}^{\mathrm{react}} + k_{dif}^{\mathrm{react}}} - \frac{k_{kin}^{\mathrm{ref}} k_{dif}^{\mathrm{ref}}}{k_{kin}^{\mathrm{ref}} + k_{dif}^{\mathrm{ref}}}\right)\frac{Vp}{W}\right] \tag{16}$$

where the upper indexes refer to the parameters of the reaction and reference flow tubes, respectively.

In the above approximation and data analysis, the OH uptake coefficient for the reference (usually inert) material is required, and in addition, the OH gaseous diffusion coefficient must be known accurately because OH reacts with the material of interest with a probability between 0.01 to unity. If the OH uptake coefficient for the reference surface and the OH diffusion coefficient are known, the radical uptake coefficient for the

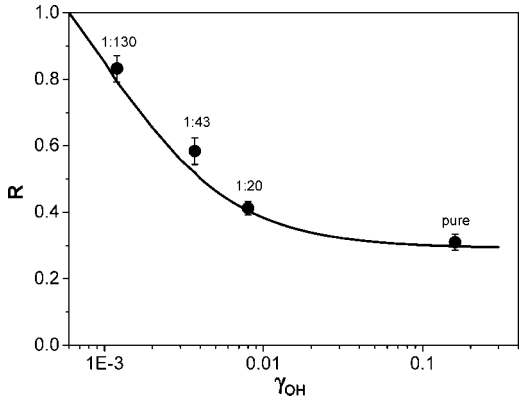

Figure 5. Predicted (solid line) and experimental (dots) dependencies of the *R* ratio for various mixtures of paraffin wax and halocarbon wax at 100 Torr. The mixing ratios of paraffin wax to halocarbon wax are given for each point.

reactive material can be determined with eq 16 by measuring the *R* ratio experimentally. Moreover, if the OH uptake coefficient is known for both the reference and reactive surfaces, eq 16 predicts the ratio *R*.

Figure 5 shows the theoretical dependence of *R* on the radical uptake coefficient of the reactive material. *R* is calculated at 100 Torr, with γ_{OH}^{ref} for an inert surface, such as halocarbon wax (series 600),[1] and $D_p = 2.1$ cm^2 s^{-1}, based on our earlier measurements for OH.[44] As seen in the figure, the R ratio is practically insensitive to the uptake coefficient in the range 0.01−1 because of the high pressure (100 Torr) used in the differential flow tube, whereas the maximum sensitivity is in the range of $(1-10) \times 10^{-3}$.

Surface Dilution Technique. At a high pressure and high uptake coefficient, the uptake is, to a large extent, controlled by diffusion. To increase the sensitivity of the VCFT method, we lowered the net uptake coefficient for the most reactive surface from a value of near unity to values of 10^{-3} to 10^{-2} using a surface dilution technique that consisted of the following steps: first, the reactive material (for example, paraffin wax) was homogeneously mixed with the inert material (halocarbon wax); both have approximately the same melting point and are miscible as liquids. Then, the glass beads were dipped into the liquid wax mixture and removed to allow the liquid to solidify on the beads. Because the average molecular weights of paraffin wax and halocarbon wax are very similar (∼600), the ratio of the number of surface active sites is considered to be equal to the weight ratio assuming that one wax molecule provides one surface active site. Therefore, a net uptake coefficient of the mixture, γ_{net}, can be estimated according to the following equation:

$$\gamma_{net} = \sum_i \alpha_i \gamma_i \qquad (17)$$

where γ_i is the uptake coefficient of an i^{th} compound in the mixture, $\alpha_i = [n_i/\Sigma n_i]$ is the fraction of an *i*th component, which meets the condition of $\Sigma_i \alpha_i = 1$, and n_i is the number of surface active sites of an *i*th component.

We studied mixtures of paraffin wax and halocarbon wax with four different ratios of 1:130, 1:43, 1:20, and pure paraffin wax which produced net OH uptake coefficient values of 0.0012, 0.0037, 0.008, and 0.16,[1] respectively. The experimentally obtained values of the *R* ratio for the paraffin wax−halocarbon wax mixtures are shown as well in Figure 5 for comparison; as seen in the figure, the experimental and theoretical values predicted on the basis of the virtual reactor approximation agree well within experimental error.

Surface dilution for salt and mineral species will be discussed further in the section on Inorganic Surfaces.

TABLE 1: Measured γ_{OH} on Organic and Soot Surfaces under Dry Conditions

surface	*R*	γ_{OH}	references
paraffin wax	0.281 ± 0.016	0.03 – 1	present work
		0.16 – 1	ref 1
pyrene	0.270 ± 0.008	0.03 – 1	present work
		0.15 – 1	ref 1
glutaric acid	0.277 ± 0.006	0.03 – 1	present work
methane-soot	0.285 ± 0.010	0.03 – 1	present work
		0.5 – 1	ref 1

Organic Surfaces. We determined the OH uptake coefficient for organic surfaces, including methane soot, under dry conditions for verification of the proposed VCFT method. First, the *R* ratio was experimentally measured and then eq 16 was applied to extract the values of k_{kin}^{react}. Subsequently, the OH uptake coefficient for the organic and methane-soot surfaces was determined using eqs 14 and 17. Results of the uptake measurements are shown in Table 1; literature values for the same organic surfaces are also shown in the table for comparison. As seen from the table, the experimental results obtained on the basis of the virtual flow tube approximation reproduce the literature values reasonably well, although the range of the measured uptake coefficient values is wider due to the decreased sensitivity of the VCFT method to high values of the uptake coefficient, as was discussed above. Meanwhile, the considerable span in γ_{OH} values (Table 1) is to a large extent due to the diffusion limitation of the uptake at 100 Torr for large γ.

The effect of water vapor on OH uptake by organic materials was studied on the pure and diluted surfaces; the organic surfaces were diluted with halocarbon wax to give a net γ_{OH} value in the region of $(1-2) \times 10^{-3}$ that corresponds to $R = 0.6-0.8$, where the sensitivity of the VCFT method is the best (see Figure 5).

In the present relative study, the surface wetting behavior of the reference halocarbon wax cannot be determined and, therefore, becomes an additional source of systematic errors. We have checked the variability of the OH uptake coefficient on halocarbon wax with relative humidity in separate experiments. These experiments, not shown here, used a fast flow tube coupled to a low-pressure CIMS with RH varying over the range of 0−24%. Results of this study showed no RH effect on radical uptake on halocarbon wax within the RH range. On the basis of these results, we can conclude that systematic errors due to uncertainties in the surface behavior of halocarbon wax under wet conditions do not exceed typical experimental errors in the present study.

Figure 6 illustrates how the surface dilution technique works. Figure 6a shows the RH dependence of *R* for pure and diluted pyrene surfaces and indicates that the ratio is independent of RH over the range 0−40%, whereas the diluted glutaric acid surface shows noticeable changes in *R* compared to the pure surface, as seen in figure 6b.

We also studied the effect of relative humidity on the *R* ratio for the diluted paraffin wax and methane−soot surfaces of known compositions. By subsequently applying eqs 16, 14, and 17, we were able to calculate the OH uptake values for the pure organic and methane−soot surfaces. The results of these experiments are shown in Figure 7. As seen in the figure, only an initially hydrophilic organic surface, such as glutaric acid,

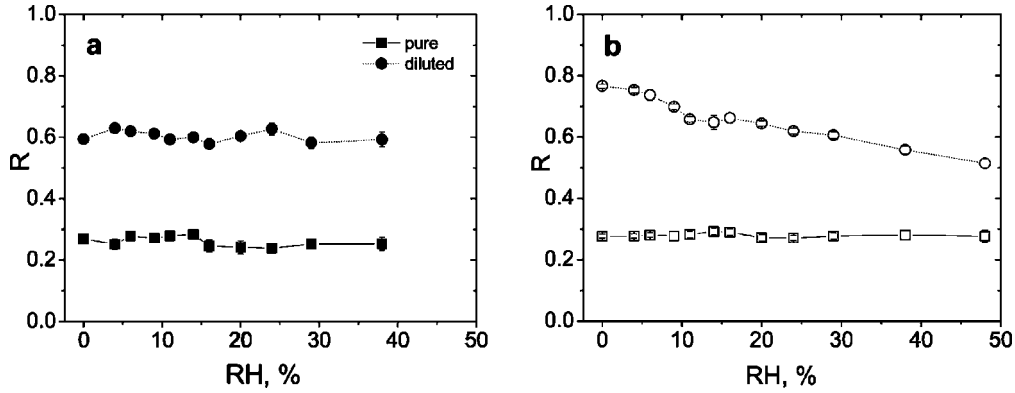

Figure 6. RH dependence of the ratio R for pure (■) and diluted (●) pyrene (a) and for pure (□) and diluted (○) glutaric acid (b) surfaces.

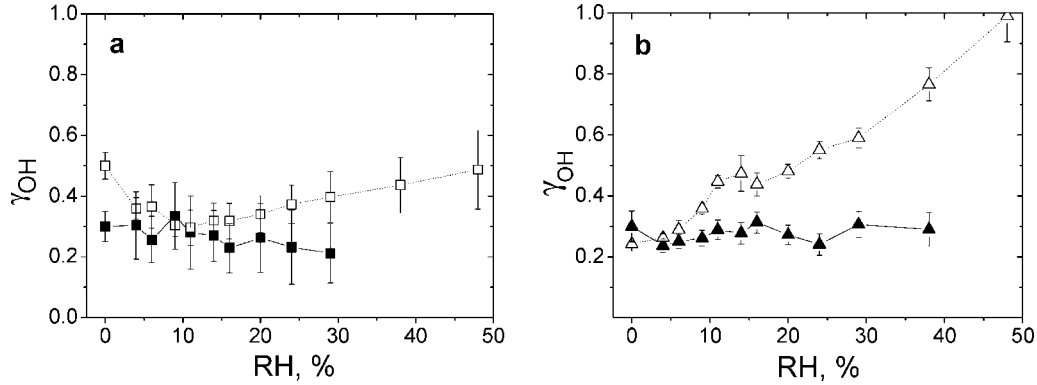

Figure 7. RH dependence of γ_{OH} for pure paraffin wax, soot (□), pyrene (μ), and glutaric acid (μ) surfaces.

shows enhancement in its reactivity toward OH, whereas for all other organic and methane−soot surfaces no noticeable changes in γ_{OH} were observed within experimental error under high humidity conditions. These results suggest that (i) OH exposure does not alter the hydrophilicity of organic and soot surfaces to an extent such that their reactivity towards OH is affected; (ii) an initially hydrophilic organic surface, with comparatively high water adsorption capacity, is able to change its reactivity by providing a different (quasi-liquid) environment for OH uptake; this can eventually lead to a change in the radical OH uptake mechanism. For example, assuming that water molecules are adsorbed mostly on hydroxyl functional groups, as more water is taken up by the surface, the degree of dissociation of glutaric acid will increase, changing the uptake mechanism to a radical−ionic one.

Reactions of OH with ions are typically faster than those with molecules.[28] An enhancement in OH uptake was observed upon the addition of H_2SO_4 to pure water.[27] This reaction proceeds via H-atom abstraction from HSO_4^-.[28] We expect a similar enhancement for organic anions like $RC(O)O^-$. Resonance stabilization of the carboxyl group results in an excess of positive charge on the α-C, weakening α-C−H bonds, and thus enhancing H-atom abstraction. Additionally, an electron transfer mechanism is plausible due to solvation of the carboxylate anion under wet conditions.

Another possible explanation for the observed enhancement of the OH uptake by glutaric acid can be the weakening of RC(O)O−H bond due to an increase in coordination number large enough to cause the partial dissociation of the surface organic diacid molecules, which in turn can result in a higher rate of H-atom abstraction.

Inorganic Surfaces. The VCFT method together with the surface dilution technique was successfully applied in the uptake experiments reported in this work for inorganic surfaces such as sea salt and mineral dust materials. However, unlike mixtures of organic surfaces with halocarbon wax, we expect inorganic/halocarbon wax surfaces to be heterogeneous at the molecular level, and therefore, it is necessary to verify that eqs 16 and 17 hold for these mixtures.

TABLE 2: Measured γ_{OH} on Inorganic Surfaces under Dry Conditions

surface	R	γ_{OH}, 10^{-3}	reference
NaCl	0.469 ± 0.012	4.6 ± 0.7	present
		4 ± 1	ref 6
$MgCl_2$	0.428 ± 0.008	6.1 ± 1.2	present
Na_2SO_4	0.523 ± 0.008	3.5 ± 0.4	present
$CaCl_2$	0.500 ± 0.015	3.9 ± 0.4	present
KCl	0.443 ± 0.010	5.5 ± 1.1	present
sea salt	0.524 ± 0.010	3.5 ± 0.4	present
		5 ± 1	ref 8

Dry Salt Surfaces. There is a very limited number of experimental studies[6–9] on OH uptake on sea salt and its components under dry conditions. We report here (see Table 2) the results of measurements of OH uptake on dry sea salt and its five major components, that is, NaCl (68%), $MgCl_2$ (14%), Na_2SO_4 (11%), $CaCl_2$ (4%), and KCl (2%); the percentages shown in round brackets represent the fraction of each component in sea salt aerosols.[47]

As can be seen in the table, the values determined with eqs 14–16 and measurements of the R ratio experimentally agree well within experimental error with the available literature data[6,8] for NaCl and sea salt, verifying that the VCFT method provides reasonably accurate values for the uptake coefficient. There are no previous literature values for $MgCl_2$, Na_2SO_4, $CaCl_2$, and KCl.

Salt Surfaces under High Humidity Conditions. The OH uptake coefficient was also determined for sea salt and the five major components under high humidity conditions using the

TABLE 3: Measured γ_{OH} on Inorganic Salt Surfaces under High Humidity Conditions[a]

	OH, 10^{-3}					
RH, %	NaCl	$MgCl_2$	Na_2SO_4	$CaCl_2$	KCl	sea salt
0	4.5 ± 0.3	5.8 ± 0.7	3.3 ± 0.3	3.7 ± 0.4	5.0 ± 0.4	3.3 ± 0.5
4	4.0 ± 0.4	5.2 ± 0.6	3.3 ± 0.2	3.3 ± 0.5	4.5 ± 0.3	2.2 ± 0.7
6	ND	5.4 ± 0.5	3.4 ± 0.2	2.9 ± 0.5	4.5 ± 0.3	2.3 ± 0.5
9	4.0 ± 0.5	6.8 ± 0.7	3.4 ± 0.2	2.7 ± 0.3	4.5 ± 0.3	2.5 ± 0.6
11	3.8 ± 0.5	7.0 ± 1.1	3.3 ± 0.2	1.7 ± 0.2	4.1 ± 0.3	3.4 ± 0.8
14	3.7 ± 0.4	7.9 ± 0.9	3.0 ± 0.2	1.4 ± 0.2	3.8 ± 0.3	4.2 ± 1.0
16	3.7 ± 0.4	8.6 ± 1.2	2.9 ± 0.2	ND	3.2 ± 0.4	4.3 ± 1.0
20	3.7 ± 0.6	9.6 ± 1.5	3.2 ± 0.2	1.2 ± 0.1	3.5 ± 0.3	5.0 ± 1.4
24	3.7 ± 0.6	8.9 ± 1.0	3.3 ± 0.2	ND	3.3 ± 0.3	5.6 ± 1.3
28	3.8 ± 0.8	8.9 ± 1.4	3.2 ± 0.2	ND	3.1 ± 0.3	6.1 ± 1.8
38	3.4 ± 1.1	ND	2.7 ± 0.2	ND	2.8 ± 0.3	8.3 ± 1.7
48	ND	ND	2.5 ± 0.3	ND	3.1 ± 0.3	ND

[a] ND: not determined or data is not available.

surface dilution technique. As mentioned above, γ was measured for the pure salt surfaces, and these values were used in eq 14 to determine k_{kin}. Additionally, the gaseous diffusion constant was calculated on the basis of previously reported data[44] and used in eq 15. These parameters were then inserted into eq 16 and used to determine γ_{net} from our experimental measurements of R. Using this method, an accurate value of α, the fraction of the salt component, is not needed but can be calculated from eq 17 if γ_{net} is known.

To verify that eq 17 holds for heterogeneous (inorganic/halocarbon wax) surfaces, we plotted the experimentally-obtained values of α for NaCl as a function of the mass of NaCl in the mixture. For relatively high dilutions, $\alpha < 0.3$, this relationship is linear within experimental error, showing that eq 17 can be applied to dilute inorganic surfaces. In the current RH studies, typical values of α did not exceed 0.3.

To relate the wetting behavior of the dilute inorganic surfaces to that of pure inorganic surfaces, we calculated α for each mixture from eq 17 and then recalculated γ for the pure inorganic surface using an α of 1. The reported values of γ at 0% RH in Table 3 were calculated in this way and agree well with the measured values of γ reported in Table 2.

Results of the uptake measurements under wet conditions are listed in Table 3; the uptake coefficient was determined by assuming that water vapor does not significantly change the surface area and morphology of these highly hygroscopic salts as long as the relative humidity is below the deliquescent point of the salt in question. As seen in the table, all the salt surfaces, except $MgCl_2$ and sea salt, showed a lowering of their reactivity by a factor between 1.3 and 3.1, whereas $MgCl_2$ and sea-salt surfaces showed the opposite behavior, indicating a notable increase in the reactivity by a factor between 1.9 and 3.8.

We can rationalize the observed changes in the OH uptake coefficient for the individual or mixed alkali−halide solid surfaces under high humidity conditions by assuming that water vapor exposure plays a crucial role in enhancing the ionic mobility of salt crystals, which in turn allows surface segregation of ions. Surface segregation is the enrichment of one component at the surface and has been observed in metal alloys and salt mixtures. According to an electronic theory developed to explain surface segregation in simple metal alloys,[48] segregation is driven by single-particle forces that depend on the particle position with respect to the inhomogeneous zeroth-order electron density in the interfacial region. As a result, segregation is more pronounced for larger species, which consistently segregate to the surface layer; the concentration profile has a maximum at the interfacial region with a thickness of a few monolayers.

Applied to wet salt surfaces, surface segregation can result in formation of a doubly charged layer near the surface (blocking of surface anions), and can also change the surface pH. Both these factors compete with each other, influencing the radical uptake in different ways, inhibiting or enhancing.

Morphology of solid alkali−halide surfaces and its subsequent changes due to water vapor exposure at humidity below the deliquescent point were extensively studied by the SEM, SPFM, and SH methods. According to these studies, a surface potential was experimentally found to be inhomogeneously distributed on a salt surface with a maximum at step edges.[49] As confirmed by these SEM and SPFM studies,[49–51] the steps on a salt surface serve as active sites for water adsorption. Upon its adsorption water can easily penetrate within the surficial region disturbing the crystal structure through creation of defects (water impurities) at concentrations proportional to relative humidity. Due to the presence of crystal defects, the ionic mobility becomes enhanced and cations move to the negatively charged surface steps. This causes reorientation of salt molecules along the interfacial region with cations facing the gas phase. Evidence for surface changes, such as formation of a more positive surface potential and a decrease in the surface anion-to-cation ratio to values less than unity at a humidity below the deliquescent point, was experimentally obtained for Br-doped NaCl, KBr, and KI surfaces in the SPFM and XPS studies.[49–51] Such reorientation of salt molecules leads to formation of a doubly charged layer in the interfacial region, which was predicted by classical molecular dynamics modeling.[52] This reorientation was studied in detail and analyzed with molecular dynamics studies;[53–55] it leads to blocking of anions on a wet salt surface making them less available for OH uptake. Assuming that anions serve as active sites for OH uptake,[20,21] the results of our uptake studies confirm indirectly the effect of anion blocking by showing a decrease in OH uptake on NaCl, $CaCl_2$, KCl, and Na_2SO_4 as the relative humidity increases. It should be mentioned that inhibition of OH uptake was observed in the present study only for salts with cations of strong bases, because they are essentially unreactive with adsorbed water molecules.

For salts with cations of weak bases, adsorbed water molecules will dissociate and react to produce cation hydroxide complexes, as in the case of Mg^{2+}, i.e.,

$$Mg^{2+} + OH^- \rightarrow MgOH^+ \qquad (18)$$

Formation of a metastable $MgOH^+$ complex was found to be thermodynamically favorable in aqueous solutions.[56,57] This hydrolysis mechanism, which results in the consumption of surface OH^-, is responsible for the lowering of surface pH (acidification) on $MgCl_2$ exposed to water vapor. These changes in the surface pH are very important for the reaction mechanism of OH uptake on NaCl proposed in chamber studies[20,21] in which the $HOCl^- + H^+$ reaction was postulated to be the rate-determining step in Cl_2 formation, thus a more acidic surface would have faster OH uptake.

The enhancement effect of lowering the surface pH, under high humidity conditions, is supported by results of the present study showing an increase in γ_{OH} for wet $MgCl_2$. Though little is known on the chemistry of the surficial layer, simple estimates based on equilibrium dissociation rate constants of H_2O and $MgOH^+$ [59–60] suggest that the surface pH of a wet $MgCl_2$ surface should be less than 7 at room temperature. On the basis of our uptake results, we can conclude that the decrease in surface pH is likely responsible for the experimentally observed enhancement in OH uptake by $MgCl_2$, and therefore, the effect of changes in surface pH becomes more important for salts with cations of weak bases.

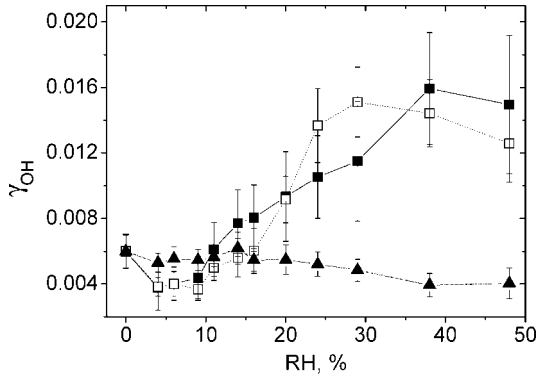

Figure 8. RH dependence of γ_{OH} for natural sea salt (■), synthetic sea salt with $MgCl_2$ (□) and without $MgCl_2$ (▲).

Sea salt is typically composed of 7−10% $MgCl_2$ by mass, a concentration that is sufficient to contribute notably to surface segregation.[50] Water-induced surface cation segregation in a mixture of NaCl and $MgCl_2$ was observed early in an XPS study.[61] Results of this experimental study indicated that an initially dry mixture of sodium and magnesium chlorides with bulk and surface composition of 9 to 1 evolves during 10 min water vapor exposure to a state with a surface composition of 1 to 1.2, whereas the bulk composition does not change significantly, suggesting that the $MgCl_2$ salt component, which has a lower deliquescence point of 38%, is efficiently concentrated at the surface. The effect of extracting the same lower deliquesced salt component was most likely observed in our uptake studies in which a wet sea-salt surface showed reactivity dependence on RH similar to that of $MgCl_2$ (Figure 8). For confirmation, the $MgCl_2$ component was removed from a synthetic sea-salt mixture, and the reactivity behavior of the mixed salt in the presence of water vapor was found to follow that of NaCl (Figure 8). It should be noted here that the contribution of other sea-salt components, such as KCl, $CaCl_2$, and Na_2SO_4, to the net sea-salt reactivity appears to be of minor importance partially due to their relatively smaller contents in the mixed salt.[51]

Mineral Dust Surfaces. Earlier laboratory studies showed that, under dry conditions, OH uptake by SiO_2 (silica) and Al_2O_3 (alumina), major components of mineral dust aerosols, is very efficient. Our uptake measurements confirmed this by measuring γ_{OH} of $(3.2 \pm 0.7) \times 10^{-2}$ for SiO_2 and of $(4.5 \pm 0.5) \times 10^{-2}$ for Al_2O_3 under the same conditions. To measure such relatively high γ_{OH} values, the surfaces were diluted with halocarbon wax to give higher CIMS sensitivity under high humidity conditions. The γ values for pure mineral dust surfaces were calculated in the same way as those for pure inorganic salt surfaces.

The γ_{OH} values measured on SiO_2 and Al_2O_3 under high humidity conditions are listed in Table 4. As seen in the table, water vapor enhances the OH uptake coefficient for both mineral oxides. Figure 9 also illustrates the observed enhancement in γ_{OH} for SiO_2 and Al_2O_3 as RH increases. The maximum observed enhancement in γ_{OH} for silica and alumina are a factor of 3 and 2, respectively, within an RH range of 0−38%.

Because the reaction mechanism of OH uptake on silica and alumina has not yet been studied in detail, we can only speculate: we assume that the OH uptake can follow the Langmuir−Hinshelwood and/or the Eley−Rideal mechanisms.[65] Both include formation of surface-bound OH, which can eventually react with either another adsorbed or gas-phase OH because the extremely strong network of covalent bonds in silica and alumina does not allow abstraction or substitution in the OH reactions with the surfaces.

TABLE 4: Measured γ_{OH} for SiO_2 and Al_2O_3 under High Humidity Conditions[a]

RH, %	γ_{OH}, 10^{-2}	
	SiO_2	Al_2O_3
0	3.2 ± 0.7	4.5 ± 0.5
	41 ± 4[62]	22 ± 11[1]
	0.2[63]	0.5[63]
		4 ± 2[64]
4	3.3 ± 0.7	4.9 ± 0.4
6	ND	5.2 ± 0.6
9	3.8 ± 0.8	5.7 ± 0.7
11	4.4 ± 1.0	7.0 ± 0.8
14	5.5 ± 1.2	7.8 ± 0.7
16	6.8 ± 1.3	7.7 ± 0.8
20	8.4 ± 1.7	7.2 ± 0.8
24	ND	8.2 ± 0.8
26	8.8 ± 2.0	ND
29	ND	8.7 ± 1.0
33	9.8 ± 2.2	ND
38	ND	8.4 ± 1.2

[a] ND: not determined or data is not available.

On the other hand, water molecules are found to be readily adsorbed on silica and alumina surfaces, causing their efficient hydroxylation upon water molecule dissociation. This leads to formation of surface H- and OH-groups, which have been detected by various spectroscopic methods.[66–71] The additional formation of Si−OH and Al−OH in the presence of water vapor most likely facilitates their reactions with adsorbed or gas-phase OH via self-reaction. Such a mechanism can explain the observed enhancement in the OH uptake rate under high humidity conditions. The products of the OH self-reaction are H_2O or H_2O_2, which can stay at the surface or can be released to the gas phase. We were unable to detect H_2O_2 in the gas phase; this could be due to the fact that H_2O_2 remains on the surface, or because of a decrease in CIMS detection sensitivity under high humidity conditions and/or slow charge transfer in the reaction of H_2O_2 with SF_6^-.

Atmospheric Implications

The results presented in this work show that the OH uptake coefficient is RH dependent both for initially hydrophilic organic surfaces and for inorganic surfaces, reaching higher values in comparison with those measured under dry conditions. These high γ_{OH} values become important for atmospheric modeling calculations in which interactions with aerosol particles are included. The mechanism of such interactions and the RH effect can vary depending on the chemical composition and the mixed state of the aerosol particles and gas-phase environment, but it

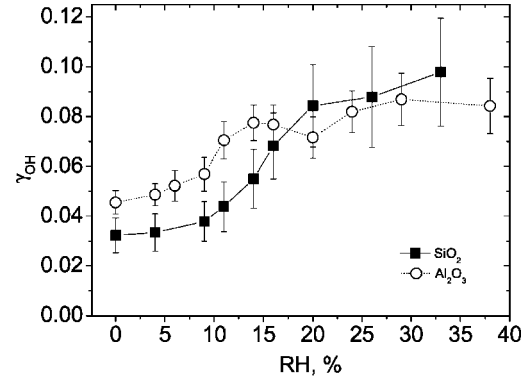

Figure 9. RH dependence of γ_{OH} for SiO_2 and Al_2O_3.

is clear that it does not change significantly the concentration level of OH in the troposphere. On the other hand, OH exposure can initiate, and be ultimately responsible for, chemical aging of atmospheric aerosol particles, modifying their physical and chemical properties. It can lead to changes in the CCN ability of aerosols and their radiative forcing as well as produce and release photochemically active gas-phase products.

The reactivity of sea salt under high humidity conditions was observed in the present study to be determined by its lower deliquescing component, such as $MgCl_2$. On the other hand, the efficiency of Cl_2 production in the reaction of OH with the deliquesced NaCl was found to be much higher than under dry conditions due to pronounced segregation of Cl^- to the surficial interface. We can therefore conclude that the presence of the $MgCl_2$ component concentrated at the sea-salt surface under subsaturated conditions will likely extend the relatively high reactivity of the sea-salt aerosol to lower relative humidity conditions increasing its contribution to Cl_2 production in the marine boundary layer.

Conclusions

An experimental study of OH uptake on surfaces of atmospheric importance has been performed under dry and high humidity conditions. Several organic and inorganic surfaces have been studied for the first time. The results of this study indicate that OH uptake is RH dependent in most cases and can reach higher values under high humidity conditions. The uptake mechanism and the RH effect on the radical capture depend on the nature of the surface and a gas-phase environment.

The results of the present study indicate that OH uptake on sea salt provides a significant contribution to Cl_2 production in the marine troposphere.

On the basis of the results we presented in this work, we can conclude that the effect of relative humidity is important and should be accounted for in atmospheric modeling studies of tropospheric aerosol chemistry.

Acknowledgment. This study was supported partially by NSF and DOE grants. J.H.P. acknowledges funding support from the Kwanjeong Educational Foundation.

References and Notes

(1) Bertram, A. K.; Ivanov, A. V.; Hunter, M.; Molina, L. T.; Molina, M. J. *J. Phys.Chem. A* **2001**, *105*, 9415.
(2) Molina, M. J.; Ivanov, A. V.; Trakhtenberg, S.; Molina, L. T. *Geophys. Res. Lett.* **2004**, *31*, L22104.
(3) Hearn, J. D.; Smith, G. D. *Geophys. Res. Lett.* **2006**, *33*, L17805.
(4) George, I. J.; Vlasenko, A.; Slowik, J. G.; Broekhuizen, K.; Abbatt, J. P. D. *Atmos. Chem. Phys.* **2007**, *7*, 4187.
(5) McNeill, V. F.; Wolfe, G. M.; Thornton, J. A. *J. Phys. Chem. A* **2007**, *111*, 1073.
(6) Gershenzon, Y. M.; Ivanov, A. V.; Kucheryavyi, S. I.; Rozenshtein, V. B. *Kinet. Catal.* **1986**, *27* (Part 1), 923.
(7) Cooper, P. L.; Abbatt, J. P. D. *J. Phys. Chem.* **1996**, *100*, 2249.
(8) Gratpanche, F.; Ivanov, A. V.; Devolder, P.; Gershenzon, Y. M.; Sawerysyn, J.-P. Uptake coefficients of OH and HO_2 radicals on material surfaces of atmospheric interest. *14th International symposium on gas kinetics a book of abstracts*; University of Leeds: Leeds, England, 1996; A12.
(9) Ivanov, A. V.; Gershenzon, Y. M.; Gratpanche, F.; Devolder, P.; Sawerysyn, J.-P. *Ann. Geophys.* **1997**, *14*, 659.
(10) Jacob, D. J. *Atmos. Environ.* **2000**, *34*, 2131.
(11) Knipping, E. M.; Lakin, M. J.; Foster, K. L.; Jungwirth, P.; Tobias, D. J.; Gerber, R. B.; Dabdub, D.; Finlayson-Pitts, B. J. *Science* **2000**, *288*, 301.
(12) Laskin, A.; Gaspar, D. J.; Wang, W. H.; Hunt, S. W.; Cowin, J. P.; Colson, S. D.; Finlayson-Pitts, B. J. *Science* **2003**, *301*, 340.
(13) Finlayson-Pitts, B. J. *Chem. Rev.* **2003**, *103*, 4801.
(14) Laskin, A.; Wang, H.; Robertson, W. H.; Cowin, J. P.; Ezell, M. J.; Finlayson-Pitts, B. J. *J. Phys. Chem. A* **2006**, *110*, 10619.
(15) Thomas, J. L.; Jimenez-Aranda, A.; Finlayson-Pitts, B. J.; Dabdub, D. *J. Phys. Chem. A* **2006**, *110*, 1859.
(16) Anastasio, C.; Newberg, J. T. *J. Geophys. Res.-Atmos.* **2007**, *112*, D10306.
(17) Keene, W. C.; Jacob, D. J.; Pszenny, A. A. P.; Duce, R. A.; Schultztokos, J. J.; Galloway, J. N. *J. Geophys. Res.-Atmos.* **1993**, *98*, 9047.
(18) Mcinnes, L. M.; Covert, D. S.; Quinn, P. K.; Germani, M. S. *J. Geophys. Res.-Atmos.* **1994**, *99*, 8257.
(19) Shaka, H.; Robertson, W. H.; Finlayson-Pitts, B. J. *Phys. Chem. Chem. Phys.* **2007**, *9*, 1980.
(20) (a) Mozurkewich, M. *J. Geophys. Res.-Atm.* **1995**, *100*, 14199. (b) Behnke, W.; Scheer, V.; Zetzsch, C. *Naturally-Produced Organohalogens*; Kluwer Academic: Drodrecht, Netherlands, 1995; Chapter 7, p 375.
(21) Oum, K. W.; Lakin, M. J.; DeHaan, D. O.; Brauers, T.; Finlayson-Pitts, B. J. *Science* **1998**, *279*, 74.
(22) (a) Knipping, E. M.; Dabdub, D. *J. Geophys. Res.-Atmos.* **2002**, *107*, 4360. (b) Knipping, E. M.; Dabdub, D. *Environ. Sci. Technol.* **2003**, *37*, 275.
(23) Frinak, E. K.; Abbatt, J. P. D. *J. Phys. Chem. A* **2006**, *110*, 10456.
(24) von Glasow, R. *Atmos. Chem. Phys.* **2006**, *6*, 3571.
(25) Pechtl, S.; von Glasow, R. *Geophys. Res. Lett.* **2007**, *34*, L11813.
(26) Chameides, W. L.; Stelson, A. W. *J. Geophys. Res.-Atmos.* **1992**, *97*, 20565.
(27) Hanson, D. R.; Burkholder, J. B.; Howard, C. J.; Ravishankara, A. R. *J. Phys. Chem.* **1992**, *96*, 4979.
(28) Buxton, G. V.; Greenstock, C. L.; Helman, W. P.; Ross, A. B. *J. Phys. Chem. Ref. Data* **1988**, *17*, 513.
(29) Gershenzon, Y. M.; Grigorieva, V. M.; Ivanov, A. V.; Remorov, R. G. *Faraday Discuss.* **1995**, *100*, 83.
(30) Takami, A.; Kato, S.; Shimono, A.; Koda, S. *Chem. Phys.* **1998**, *231*, 215.
(31) Vieceli, J.; Roeselova, M.; Potter, N.; Dang, L. X.; Garrett, B. C.; Tobias, D. J. *J. Phys. Chem. B* **2005**, *109*, 15876.
(32) Prinn, R. G.; Huang, J.; Weiss, R. F.; Cunnold, D. M.; Fraser, P. J.; Simmonds, P. G.; McCulloch, A.; Harth, C.; Salameh, P.; O'Doherty, S.; Wang, R. H. J.; Porter, L.; Miller, B. R. *Science* **2001**, *292*, 1882.
(33) Smith, S. C.; Lee, J. D.; Bloss, W. J.; Johnson, G. P.; Ingham, T.; Heard, D. E. *Atmos. Chem. Phys.* **2006**, *6*, 1435. (a) Bahm, K.; Khali, M. A. K. *Chemosphere* **2004**, *54*, 143.
(34) Seinfeld, J. H.; Pandis, S. N. *Atmospheric chemistry and physics: From air pollution to climate change*; John Wiley & Sons, Inc.: New York, 1998; p 1326.
(35) *CRC Handbook of Chemistry and Physics* 88th ed.; CRC Press: Boca Raton, FL, 2007.
(36) Buldakov, M. A.; Cherepanov, V. N. *J. Phys. B* **2004**, *37*, 3973.
(37) Zuberi, B.; Johnson, K. S.; Aleks, G. K.; Molina, L. T.; Laskin, A. *Geophys. Res. Lett.* **2005**, *32*, L01807.
(38) Hemminger, J. C. *Int. Rev. Phys. Chem.* **1999**, *18*, 387.
(39) DeMore, W. B.; Sander, S. P.; Howard, C. J.; Ravishankara, A. R.; Golden, D. M.; Kolb, C. E.; Hampson, R. F.; Kurylo, M. J.; Molina, M. J. *Chemical Kinetics and Photochemical Data for Use in Stratospheric Modeling*; Evaluation Number 12, JPL Publication 97-4; NASA Jet Propulsion Laboratory, Pasadena, CA, 1997.
(40) Atkinson, R.; Baulch, D. L.; Cox, R. A.; Crowley, J. N.; Hampson, R. F.; Hynes, R. G.; Jenkin, M. E.; Rossi, M. J.; Troe, J. *Atmos. Chem. Phys.* **2004**, *4*, 1461.
(41) Harrison A. G. In *Chemical ionization mass spectrometry*, 2nd ed.; CRC Press: Boca Raton, FL,1992; p 208.
(42) Wickramanayake, P. P.; Gardner, G. J.; Michael Siu, K. W.; Berman, S. S. *Int. J. Mass Spectrom. Ion Proc.* **1986**, *69*, 39.
(43) Arnold, S. T.; Viggiano, A. A. *J. Phys. Chem. A* **2001**, *105*, 3527.
(44) Ivanov, A. V.; Trakhtenberg, S.; Bertram, A. K.; Gershenzon, Y. M.; Molina, M. J. *J. Phys. Chem. A* **2007**, *111*, 1632.
(45) Zasypkin, A. Y.; Grigorieva, V. M.; Korchak, V. N.; Gershenzon, Y. M. *Kinet. Catal.* **1997**, *38*, 772.
(46) Seinfeld J. H., Pandis S. N. *Atmospheric Chemistry and Physics*; Wiley-Interscience: New York, 1998.
(47) Lin, T. F.; Gilbert, J. B.; Naggar, J. A.; Imblum, T. M. *Proc. IEEE OCEANS' 91, Honolulu, Hawaii* **1991**, *3*, 1629.
(48) Barnett, R. N.; Landman, U.; Cleveland, C. L. *Phys. Rev. B* **1983**, *28*, 6647.
(49) Ghosal, S.; Verdaguer, A.; Hemminger, J. C.; Salmeron, M. *J. Phys. Chem. A* **2005**, *109*, 4744.
(50) Ghosal, S.; Shbeeb, A.; Hemminger, J. C. *Geophys. Res. Lett.* **2000**, *27*, 1879.
(51) Ghosal, S.; Hemminger, J. C.; Bluhm, H.; Mun, B. S.; Hebenstreit, E. L. D.; Ketteler, G.; Ogletree, D. F.; Requejo, F. G.; Salmeron, M. *Science* **2005**, *307*, 563.
(52) Jungwirth, P.; Tobias, D. J. *J. Phys. Chem. B* **2002**, *106*, 6361.
(53) Ishiyama, T.; Morita, A. *J. Phys. Chem. C* **2007**, *111*, 721.
(54) Ishiyama, T.; Morita, A. *J. Phys. Chem. C* **2007**, *111*, 738.
(55) Ishiyama, T.; Morita, A. *J. Phys. Chem. A* **2007**, *111*, 9277.

(56) Wagman, D.; Evans, W.; Purker, V.; Schumm, R.; Halow, I.; Baylor, S.; Churney, K.; Nutall, R. *J. Phys. Chem. Ref. Data* **1982**, *11*, Suppl. 2.

(57) Chase, M. W., Jr.; Davies, C. A.; Downey, J. R., Jr.; Frurip, D. J.; McDonald, R. A.; Syverud, A. N. *JANAF thermochemical tables*, 3rd ed., 1985; Vol. 14, Suppl. 1.

(58) Linke, W. F. In *Solubilities inorganic and metal-organic compounds*, 4th ed.; American Chemical Society: Washington, DC, 1965.

(59) Stock, D. I.; Davies, C. W. *Trans. Faraday. Soc.* **1948**, *44*, 856.

(60) Harris, D. C. In *Quantitative chemical analysis*, 3rd ed.; W. H. Freeman and Co.: New York, 1991.

(61) Dementiev, A. P.; Zelenov, V. V.; Aparina, E. V.; Shestakov, D. V.; Iliin, S. D.; Gershenzon, Y. M. *Khim. Fiz.* **2004**, *23*, 54.

(62) Bogart, K. H. A.; Cushing, J. P.; Fisher, E. R. *J. Phys. Chem. B* **1997**, *101*, 10016.

(63) Suh, M.; Bagus, P. S.; Pak, S.; Rosynek, M. P.; Lunsford, J. H. *J. Phys. Chem. B* **2000**, *104*, 2736.

(64) Gershenzon, Y. M.; Ivanov, A. V.; Kucheryavyi, S. I.; Rozenshtein, V. B. *Kinet. Katal.* **1986**, *27*, 1069.

(65) Steinfeld, J. I.; Francisco, J. S.; Hase, W. L. In *Chemical Kinetics and Dynamics*, 2nd ed.; Prentice Hall: Upper Saddle River, NJ, 1998.

(66) Schaefer, J. A.; Stucki, F.; Frankel, D. J.; Göpel, W.; Lapeyre, G. J. *J. Vac. Sci. Technol. B* **1984**, *2*, 359.

(67) Nishijima, M.; Edamoto, K.; Kubota, K.; Tanaka, S.; Onchi, M. *J. Chem. Phys.* **1986**, *84*, 6458.

(68) Chen, J. G.; Crowell, J. E.; Yates, J. T. *J. Chem. Phys.* **1986**, *84*, 5906.

(69) Thiel, P. A.; Madey, T. E. *Surf. Sci. Rep.* **1987**, *7*, 211.

(70) Elam, J. W.; Nelson, C. E.; Cameron, M. A.; Tolbert, M. A.; George, S. M. *J. Phys. Chem. B* **1998**, *102*, 7008.

(71) Fu, Q.; Wagner, T.; Rühle, M. *Surf. Sci.* **2006**, *600*, 4870.

JP8012317